Thermodynamics and structure of hydrogen, methane, argon, oxygen, and carbon dioxide adsorbed on single-wall carbon nanotube bundles

M. Bienfait,[1] P. Zeppenfeld,[2,*] N. Dupont-Pavlovsky,[3,†] M. Muris,[1,‡] M. R. Johnson,[4] T. Wilson,[5] M. DePies,[5] and O. E. Vilches[5]

[1]*CRMC2-CNRS, Faculté de Luminy, Case 901, F-13288 Marseille Cedex 9, France*
[2]*Institut für Experimentalphysik, Johannes Kepler Universität Linz, A-4040 Linz, Austria*
[3]*LCSM, Université H. Poincaré, BP 239, F-54506 Vandoeuvre les Nancy Cedex, France*
[4]*Institut Laue-Langevin, BP 156, F-38042 Grenoble Cedex 9, France*
[5]*Department of Physics, University of Washington, Seattle, Washington 98195-1560, USA*

(Received 22 January 2004; published 19 July 2004)

Adsorption isotherms, isosteric heats of adsorption, and neutron diffraction measurements of hydrogen, methane, argon, oxygen, and carbon dioxide adsorbed on single-wall carbon nanotube bundles show that all species, except CO_2, condense first on high-energy binding sites, such as the grooves and the widest interstitial channels, and then on the outer rounded surface of the bundles. As for CO_2, only one set of adsorption sites is observed, which is attributed mainly to the grooves. The diffraction results further reveal that the average packing of the bundles is not changed upon adsorption and that no significant overall bundle dilation is observed on our sample. Molecular dynamic simulations confirm and complete our interpretation.

DOI: 10.1103/PhysRevB.70.035410 PACS number(s): 61.48.+c, 68.43.Fg, 61.12.Ld, 68.47.−b

I. INTRODUCTION

Much attention has been focused in the last five years on the exciting possibilities for one-dimensional (1D) and two-dimensional (2D) adsorption of many substances on closed-end single-wall carbon nanotube bundles (SWNTBs).[1–26] Carbon nanotubes are made of graphene sheets wrapped around themselves into tubes with a diameter of 1−2 nm and a length of a few μm. For our study and in this paper, we consider only tubes that are capped at both ends and are hexagonally packed in bundles with a typical diameter of about 10 nm. SWNTBs exhibit linear arrays of adsorption sites, thus providing a substrate for the physical realization of 1D matter of physisorbed atoms or molecules. The 1D adsorption sites are located in the interstitial channels (IC) between the tubes within a bundle and in the grooves (G) separating two adjacent tubes on the outer surface of a bundle. In addition, 2D-like sites are located on the graphene outer surface (S). The questions that have been addressed to date are: (i) Where and in what quantities do the gases adsorb on the SWNTBs? (ii) What are the thermodynamic and structural properties of the adsorbates? (iii) How does the adsorption modify the structure of the bundles?

Partial answer to these questions have been given in the literature[7–13,15,16,20] and previous work of our group.[2,6,14,26] Based on the results of these studies the following adsorption scenario has been proposed: adsorption starts as linear chains at the strongest binding energy sites, namely the grooves between adjacent nanotubes on the outside surface of the bundles and some larger, accessible interstitial channels in the interior of the bundles. After these sites are filled, adsorption proceeds on the external surface of the nanotube bundles. It has been predicted theoretically,[18] and inferred from adsorption isotherms,[15] that the 2D adsorbate structure on the external bundle surface initially builds up adjacent to the occupied grooves until the entire external surface is covered by a single monolayer. The binding energies measured for this later stage of adsorption are comparable but somewhat smaller than for adsorption on the basal plane of graphite, whereas the binding energy is considerably larger on the preferential adsorption sites (G, IC) populated during the initial stage of adsorption.

The aim of this paper is to check whether the above scenario is generally valid for the many gases studied so far and to establish characteristic trends. To this end, we combine thermodynamic data with neutron diffraction results. We have selected several molecular and atomic species (hydrogen, methane, argon, oxygen, and carbon dioxide) for technical and practical reasons. In particular, these substances have isotopes with large neutron coherent cross sections. In addition, they were chosen because certain specific properties or applications could be anticipated. For instance, hydrogen adsorption on SWNTBs was thought to have potential application in gas storage[21,22] or could be used for quantum sieving.[23,24] Furthermore, a 1D liquid-solid transition was predicted to occur at very high linear densities.[25] The thermodynamics of methane adsorption has been studied extensively.[2,11,14,16] It was tempting to complement these studies by neutron diffraction measurements using the deuterated methane molecule CD_4 to obtain structural information for this adsorbate. Recent calculations[17] predict that if rare gas atoms like Ar can enter the interstitial channels separating perfect monodisperse nanotubes, then they will slightly dilate the bundle lattice by about 0.33 Å, which corresponds to 2% of the average distance of 17 Å between adjacent nanotubes in the bundle. Antiferromagnetic order of O_2 adsorbed as a 2D overlayer on graphite was observed several years ago.[27–32] It is interesting to explore whether this order persists on the external surface of the bundles or even along the chains adsorbed in the grooves or inside the interstitial channels. In addition, it was suggested that SWNTBs could be used as a highly susceptible oxygen sensor.[33,34] Fi-

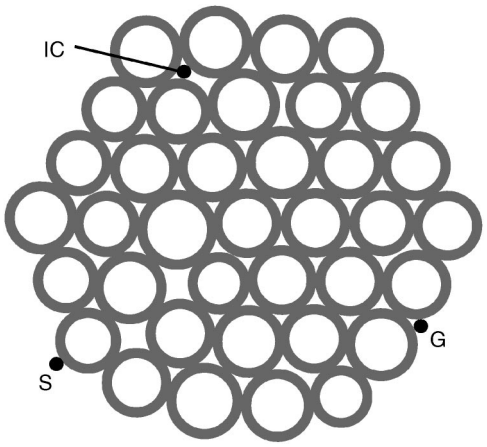

FIG. 1. Schematic section of a nanotube bundle containing 37 nanotubes with a diameter of (17 ± 1)Å. The dispersion of the nanotube diameter gives rise to an imperfect lateral ordering and heterogeneous interstitial channels (IC) providing possible adsorption sites for atoms and small molecules (black dots drawn to the size of a particle with 4 Å diameter). Other adsorption sites are the grooves (G) and the rounded outer surface of the bundle (S).

nally, CO_2 is an elongated molecule exhibiting a sizeable quadrupolar moment. It has been shown that CO_2 does not adsorb on graphite below 104 K[35] and that, above this temperature, only a single layer is stable. Further adsorption leads to the formation of 3D clusters. The question is whether this nonwetting behavior is also reflected in the adsorption properties of CO_2 on SWNTBs.

Several preliminary reports combining thermodynamic and neutron diffraction data for methane,[5,36] hydrogen,[5,6] and Ar[26] have been published. Here we want to compare all the results obtained so far by our group and answer, at least partly, the questions raised in this introduction. The paper is organized as follows. First the thermodynamic measurements are reported and analyzed. Then, the neutron diffraction data are described and compared to computer simulations.

II. EXPERIMENTAL

Our adsorption cells were made of aluminum (neutron diffraction) and glass or silica (adsorption isotherms) containing a powder of SWNTB provided by the GDPC Laboratory of the University of Montpellier.[37,38] The nanotubes were prepared by an yttrium-nickel catalyzed electric arc discharge in a helium atmosphere. This method produces nanotubes closed at both ends. Amorphous and graphitized carbon and metal particles embedded in carbon are also present in the sample and can be easily identified in the neutron diffraction spectra. A few nanotubes are isolated, but most are associated in bundles comprising 30–50 individual tubes parallel to each other in a hexagonal arrangement. The distance between two adjacent tubes in a bundle is 17 Å on average, with a slight dispersion of the tube diameters of the order of ±1 Å.[38,39] This dispersion likely produces a distribution in width and shape of the interstitial channels, as indicated schematically in Fig. 1.

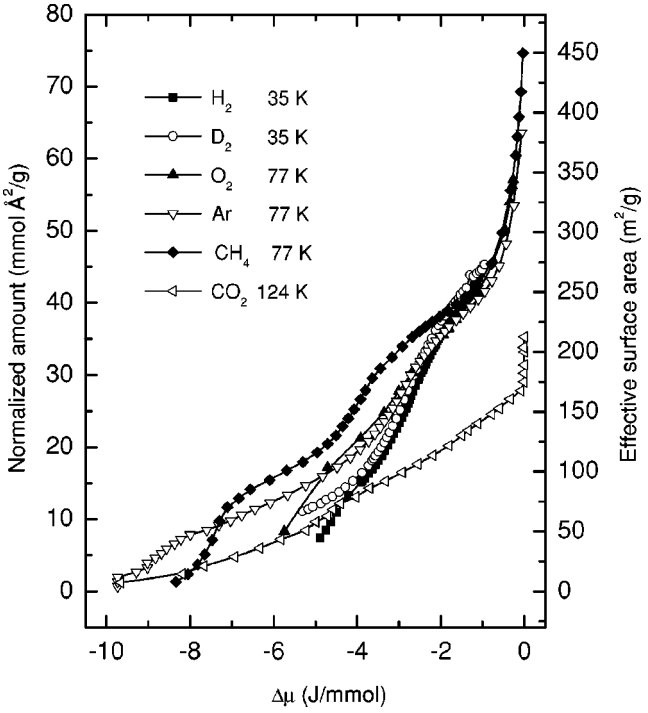

FIG. 2. Adsorbed amounts of H_2, D_2, O_2, Ar, CH_4, and CO_2 on SWNTBs, normalized to the respective monolayer density on graphite and to 1 g of the SWNTB sample, as a function of the chemical potential relative to the bulk chemical potential at the same temperature. Two risers are observed for all gases except for CO_2. The first riser corresponds to high energy adsorption sites (grooves and the widest interstitial channels, see Fig. 1). The second riser (lower binding energy) is assigned to adsorption on the curved graphene sheets forming the outer surface of the bundles.

A. Thermodynamics

Two kinds of thermodynamic measurements were performed. Adsorption isotherms were recorded by the volumetric method[2,14] after outgasing the sample at 200 °C (glass cell) or 600 °C (silica cell) for several hours. Isothermal calorimetry at 77.4 K was carried out after outgasing at 400 °C.[2] Here we do not want to duplicate the adsorption isotherms published previously,[2,14] but rather give a concise presentation (Fig. 2) of the adsorbed amount (coverage) of H_2, D_2, CH_4, Ar, O_2, and CO_2 as a function of the chemical potential $\Delta\mu = RT\ln(p/p_0)$ where p is the equilibrium pressure of the gas surrounding the SWNTBs, and p_0 is the bulk vapor pressure at the temperature at which the measurement was taken. In addition, we report results of the isosteric heats of adsorption q_{st} for the same gases as a function of the adsorbed amount (Fig. 3). q_{st} was obtained from either of the two types of thermodynamic measurements mentioned above. In the first case, a series of adsorption isotherms was recorded at different temperatures, and $q_{st} = -Rd(\ln p)/d(1/T)$ was determined from the slope of the Clausius-Clapeyron plot. Alternatively, isothermal calorimetry directly yields the differential heat of adsorption q_{diff} as a function of coverage.[40] The two heats of adsorption are related by a simple relation:[41] $q_{st} = q_{diff} - RT$. A summary of the various heats of adsorption and vaporization of the different gases is given in Table I.

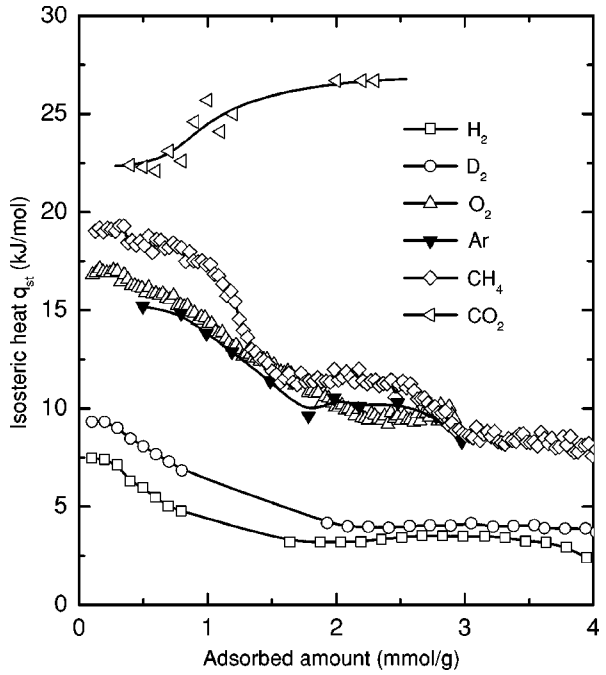

FIG. 3. Isosteric heat of adsorption q_{st} as a function of coverage (total adsorbed amount). The data for CH_4 and O_2 were obtained by isothermal calorimetry and for the other adsorbates by adsorption isotherm measurements. Solid lines are guides to the eye. The two plateaus for H_2, D_2, O_2, Ar, and CH_4 correspond to the two risers in Fig. 2. For large doses q_{st} tends towards the latent heat of vaporization q_{3D} (see Table I).

Figure 2 exhibits two risers of the adsorbed amount for H_2, D_2, O_2, Ar, and CH_4, but only a single one for CO_2. This last molecule clearly can bind in fewer adsorption sites than the other molecules, indicating that the adsorption mechanism is, indeed, different for CO_2. Note that the amounts in Fig. 2 are normalized to the monolayer density of the respective species adsorbed on the basal plane of graphite, namely: 0.094 $Å^{-2}$ for H_2,[42,43] 0.099 $Å^{-2}$ for D_2,[42,43] 0.085 $Å^{-2}$ for O_2,[27] 0.080 $Å^{-2}$ for Ar,[44] 0.066 $Å^{-2}$ for CH_4,[45] and 0.064 $Å^{-2}$ for CO_2.[35] The total amounts condensed when the major part of the adsorption sites are covered ($\Delta\mu \sim -2$ J/mmol) scale with the molecular area at monolayer completion on graphite except for the case of CO_2. For the former species, the normalized amount corresponds to an "effective" covered area (assuming the monolayer density on graphite) of the order of 250 m^2 per 1 g of the SWNTB sample. In the case of CO_2, the normalized amount is only about 60% of this value, which is again indicative of a different adsorption behavior for CO_2.

TABLE I. Isosteric heats of adsorption (kJ/mol) for various gases adsorbed on SWNTBs in highly binding sites (q_1, first plateau in Fig. 3) and on the external surface of the bundle (q_2, second plateau in Fig. 3). For comparison, the isosteric heat for monolayer adsorption on the basal plane of graphite, q_{Gr}, and the 3D heats of vaporization, q_{3D}, are also given.

	q_1	q_2	q_{Gr}	q_{3D}
H_2	~7.5[6]	3.3[6]	4.2[48]	0.9[51]
D_2	~9.4[6]	4.0[6]	4.4[48]	1.3[51]
CH_4	~18.3	11.3	14.9[2]	8.2
Ar	~15[6]	10.0[6]	10–12[40]	6.5
O_2	~16	10.0	10–13[49], 12[50]	6.9
CO_2	~22.5		25.3–22.7[35]	26.7[35]

The first riser in Fig. 2 (corresponding to the first plateau in Fig. 3) occurs at relatively small chemical potential (ranging between −8.8 J/mmol for Ar and −4.8 J/mmol for H_2). The position of these first risers reflects the adsorption energy of the most strongly binding sites on the SWNTBs in relation to those in the 3D bulk. These sites are mainly located in the grooves on the external surface of the bundles (G in Fig. 1).[8,12,14,16,19] However, their relative abundance is not large enough to account for the quantities adsorbed across the first riser. In fact, the ratio of the amounts adsorbed during the first and second riser, respectively, can be extracted from Fig. 2 and is found to be of the order of 1:1 to 1:2. This value should be compared to the relative number of sites in the grooves and those on the remaining rounded parts of the outer surface. For a hexagonal arrangement of 17 Å diameter tubes this ratio is 1:5 to 1:6, depending on the molecule size[19] and, hence, clearly smaller than the experimental value. This suggests that there are more "strongly binding sites" than just the central grooves and that other adsorption sites, some of them probably located in the widest interstitial channels (IC in Fig. 1), must be populated during the initial adsorption stage (first riser in Fig. 2). Indeed, adsorption energy calculations show that in real bundles exhibiting a distribution of interstitial channel widths, the widest channels have binding energies equal or larger than the groove sites.[36,46]

The second riser for H_2, D_2, O_2, Ar, and CH_4 occurs at about the same reduced chemical potential $\Delta\mu$. This corresponds to adsorption energies (see Table I) smaller by about 20%–30% as compared to the respective monolayers adsorbed on graphite. These lower binding sites are located on the rounded part of the outer bundle surfaces. There is a general agreement on this point[2,16,20] because the adsorption energy on a single, graphite plane (graphene sheet) is certainly smaller than on a graphite semi-infinite crystal. Furthermore, the convex curvature of the outer surface also tends to reduce the adsorption energy.[47] The isosteric heat of adsorption q_{st} as a function of the adsorbed amount represented in Fig. 3 exhibits the same behavior for H_2, D_2, O_2, Ar, and CH_4, namely a high-energy plateau corresponding to adsorption in the grooves, the widest interstitial channels, and some other high-binding energy sites, followed by a second plateau corresponding to adsorption on the outer graphene surfaces, and a final decrease at large coverage to reach the value of the heat of vaporization (multilayer condensation) indicated in Table I. Note that our results are in agreement with the isosteric heats q_{st} reported for a limited number of coverages by others groups for CH_4 (Ref. 16) and O_2.[50] They are also in fairly good agreement with calculations for CH_4[36,46] and Ar.[46] In addition, the measured values of the chemical potential and of the isosteric heat of adsorption for H_2 and D_2 are quite consistent with the quantum sieving predicted for hydrogen isotopes.[23,24] For instance, at

TABLE II. Total adsorbed amounts (in mmol/g) of the various gases for which diffraction spectra have been recorded. Also given are the temperature T_{intro} at which the gas was introduced into the cell and the temperature T_{meas}, at which the diffraction spectra were recorded.

	Coverage mmol/g	T_{intro} K	T_{meas} K
CD_2	0.9, 1.4, 2.4, 2.9	70	70
D_2	0.2, 0.4, 0.9, 1.4, 2.2, 3, 3.9	60[a], 40[b]	10
At	0.3, 0.7, 2.7	100[a], 70[b]	40
O_2	0.8, 1.7, 4.7	70[a], 60[b]	2, 18, 30, 40
CO_2	0.8	130	130

[a]Low coverage.
[b]High coverage.

35 K for our real heterogeneous SWNTB sample, the vapor pressure of D_2 is about one order of magnitude smaller than for H_2, a value to be compared to the factor of 20 between HT and H_2 calculated for the same temperature and homogeneous SWNTBs of the same diameter.

The adsorption behavior of the CO_2 molecule is quite different because only a small initial plateau is observed in Fig. 3. Note that the corresponding values for q_{st} are smaller than the heat of vaporization of bulk CO_2. This shows that the adsorbate is stabilized by entropic effects.[35] As already recalled in the Introduction, CO_2 is not strongly attracted by the graphite surface (the adsorbed layer is unstable below 104 K), and it should be even less attracted by a single graphene sheet. We propose to assign the initial plateau in Fig. 3 to adsorption in the grooves and in some of the interstitial channels, but the thermodynamic data by themselves do not allow to be conclusive on this point.

The next section deals with neutron diffraction experiments after adsorption of the various gases on our SWNTB sample. These studies are intended to provide structural information on the adsorbed species. They should also answer the remaining questions left open by the thermodynamic experiments.

B. Neutron diffraction

1. Diffraction patterns

The diffraction experiments were performed on the 660-mg SWNTB sample used previously for inelastic neutron scattering studies of CH_4[3,4] and neutron diffraction measurements on CD_4, D_2,[5] and Ar.[26] The sample was outgassed at 150 °C for one day prior to the experiments. Several doses (coverages) as listed in Table II were investigated, in order to explore the whole range of adsorption energies of the different gases. The adsorbates were slowly introduced into the sample cell over a time period of about one hour at temperatures for which the pressure could be controlled during the major part of the adsorption. The introduction temperatures are indicated in Table II and were usually different for low and high coverages. The temperature was then slowly adjusted to the measurement temperature also reported in Table II. The recording of the neutron diffraction patterns was started when equilibrium was reached—typically after one hour—and the total measuring time was of the order of 10 hours per coverage. Most of the experiments were performed on the D20 diffractometer at the Institut Laue Langevin (ILL) in Grenoble, using a wavelength $\lambda = 2.414$ Å and a scattering vector range $0.2\ \text{Å}^{-1} < Q < 5\ \text{Å}^{-1}$. A few experiments were also performed on the D1B diffractometer at the ILL, with $\lambda = 2.527\ \text{Å}^{-1}$. The results obtained on both instruments were similar and reproducible, with higher quality data and larger Q-range obtained on D20. Neutron diffraction spectra were recorded from the bare SWNTB sample and after adsorption of the different doses listed in Table II. A typical example is represented in Fig. 4(a) for 2.7 mmol/g of adsorbed ^{36}Ar. The patterns reveal the diffraction lines of the SWNTBs, the cell, the cryostat, and the changes induced upon adsorption. The features at wave vector transfer $Q = 0.42$, 0.73, 0.85, and 1.1 Å^{-1} result from the hexagonal medium-range order of the tubes within the bundles with a periodicity of about 17 Å (see Fig. 1) and correspond to the (10), (11), (20), and (21) Bragg reflections from the bundle lattice, respectively [dotted lines in Fig. 4(a)]. Some of the structures at about 3 Å^{-1} arise from the long-range order along the nanotubes in the

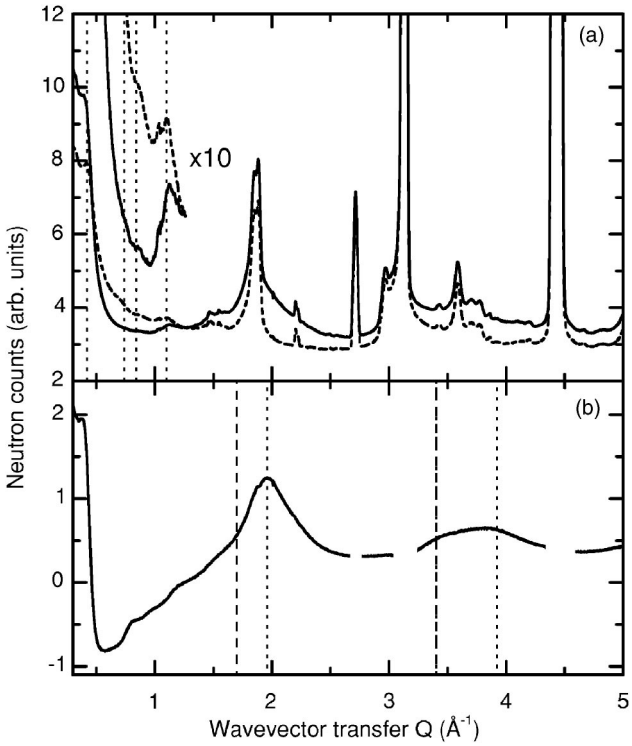

FIG. 4. (a) Neutron diffraction spectra of the bare SWNTB sample (broken line) and upon adsorption of 2.7 mmol/g (solid line) of ^{36}Ar. The dotted lines indicate the positions of the Bragg diffraction peaks expected for a hexagonal packing of the tubes within the bundles with a lattice spacing of about 17 Å. (b) Difference between the diffraction spectra in (a), revealing the changes induced upon adsorption. The vertical lines indicate the peak positions expected for Ar condensed in linear chains (dashed lines) and in 2D hexagonal arrays (dotted lines).

bundles.[38] In addition, many extra peaks are due to impurities in the substrate, e.g., those between 1.8 and 1.9 $Å^{-1}$ from graphitized carbon, those at 3.1 and 3.6 $Å^{-1}$ from Ni, at 2.7 and 3.1 $Å^{-1}$ from the aluminum container, and the 4.45 $Å^{-1}$ line from Al_2O_3. The changes upon adsorption are most evident in the difference spectrum (^{36}Ar on bundles minus bare bundles) shown in Fig. 4(b): (i) An increase of the intensity of the 0.42 $Å^{-1}$ peak can be observed. A detailed analysis shows that its position also shifts towards lower Q-values for large coverages. This will be discussed in Sec. II B 2. (ii) A marked decrease of the intensity is observed between 0.5 and 1.2 $Å^{-1}$. This drop arises from a cross-interference between the nanotubes and the atoms or molecules adsorbed in the interstitial channels as already outlined in Ref. 13 and between the nanotubes and the adsorbed species on the outer surface of the bundle (groove sites and graphene surface) as shown in recent simulations.[36] (iii) Finally, two broad peaks associated with the diffraction from the adsorbate (either 1D chains or 2D patches) can be seen, one between 1.5 and 2.4 $Å^{-1}$ and the other between 3 and 4.5 $Å^{-1}$.

The same general trend is observed for different doses of the other adsorbed gases as shown in Figs. 5(a)–5(e) for Ar, CD_4, D_2, O_2, and CO_2, respectively. In all cases, the intensity of the broad diffraction feature centered around 2 $Å^{-1}$ increases with the adsorbed amount, except for CO_2 for which only one dose has been studied. At the same time, the peak position shifts upward by about 10% from low to high coverages, indicating that the *average* lattice spacing of the adsorbate decreases with coverage by the same amount. This apparent compression is considerably larger than expected for these gases (except D_2) and contrasts the much weaker compression observed upon adsorption of the same species on the basal plane of graphite. We will see below that we can interpret these data by considering two contributions [centered at the positions indicated by the vertical lines in Fig. 4(b)] to each of the broad diffraction features: one from linear chains with an average periodicity a (reciprocal lattice spacing $Q_1=2\pi/a$), the other from pseudo-hexagonal patches giving rise to reciprocal lattice spacing $Q_2=4\pi/(\sqrt{3}a)$. Then, the relative weight of the hexagonal patches at Q_2 ($\sim$1.95 $Å^{-1}$ for Ar) simply increases compared to the linear chains at Q_1 ($\sim$1.7 $Å^{-1}$ for Ar) with increasing coverage. This is consistent with the filling, first, of the grooves and of the widest interstitial channels (1D adsorbate chains) and, second, of the curved outer bundle surfaces (2D hexagonal patches). A detailed peak shape analysis is presented in Sec. II C.

Two adsorbates D_2 and O_2 merit special attention. As mentioned in the Introduction, a one-dimensional liquid-solid transition was predicted (at $T=0$ K) for H_2 at very high linear densities.[25] No indication of such a transition was found for D_2 in the large range of coverages (from 0.2 to 3.9 mmol/g) studied in this work. This may be due to the presence of a finite size distribution of nanotube diameters in our sample as opposed to the idealized situation assumed in the calculations. As for O_2, the run with 4.7 mmol/g was studied carefully as the temperature was raised. At this coverage the external bundle surface is covered by a complete monolayer plus a few more mmol/g

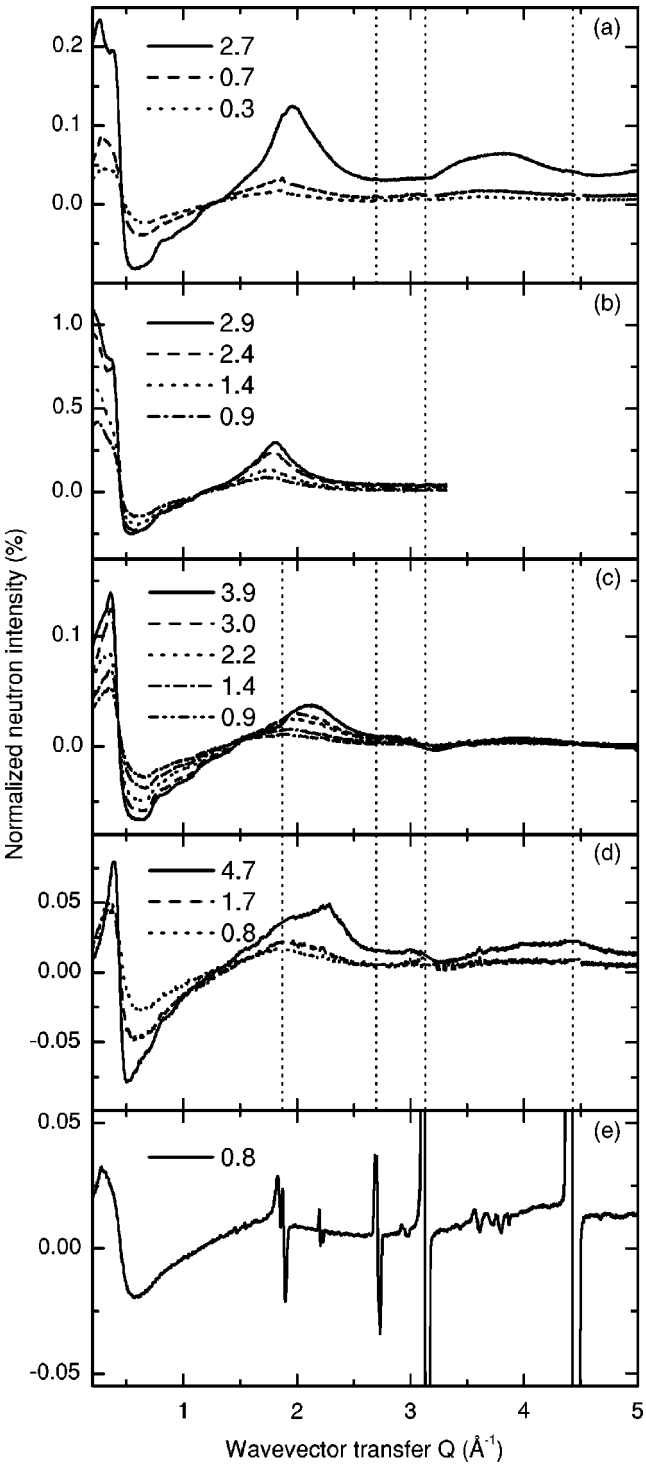

FIG. 5. Diffraction difference spectra (after subtraction of the bare SWNTB spectrum) for several doses (as given in mmol/g in the legends) for Ar (a), CD_4 (b), D_2 (c), O_2 (d), and CO_2 (e). Sharp double-spiked features, particularly apparent in (e), arise from the contributions of catalyst, cell, and amorphous carbon. Dotted lines indicate the positions where spurious peaks arising from a poor background subtraction of these contributions have been removed from the spectra in (a)–(d).

which should allow to compress it into the 2D magnetic phase. We found that the adlayer melted between 30 and 40 K, as expected for O_2 on graphite.[27,31,32] At low temperature, however, we only observed a broad diffraction peak consistent with the two 2D peaks at 2.18 and 2.32 $Å^{-1}$ known from adsorption on graphite.[30,31] There was no sign of magnetism, such as a superstructure peak at 1.2 $Å^{-1}$ characteristic of the antiferromagnetically ordered phase.[30,31] The diffraction patterns recorded at 2 K for lower O_2 coverages did not show any sign of magnetic ordering either. The diffraction pattern of CO_2 [Fig. 5(e)] is poorly defined and does not bring enough structural information to confirm the location of the molecules in the grooves. This issues can be solved with the help of molecular dynamics calculations along the same lines as described in Ref. 36. Indeed, the adsorption energy of CO_2 is found to be 27.7 kJ/mol in the grooves and 14.0 kJ/mol on the graphene surface, hence favoring molecules mainly in the groove sites.

2. Apparent bundle dilation

As recalled in the Introduction, a dilation of the bundle lattice section was expected if molecules adsorb inside the interstitial channels. On the other hand, previous theoretical calculations by Stan *et al.* predict stronger binding to G sites than to IC sites, even if dilation of the bundles is allowed.[17] For the case of Ar, we performed a contrast neutron diffraction experiment by using two Ar isotopes, namely ^{36}Ar with a large coherent cross section (σ=77.9 barn) versus ^{40}Ar, which is almost invisible for neutrons (σ=0.42 barn). If the SWNTB skeleton is dilated upon ^{40}Ar adsorption it should be seen on the bundle diffraction peaks, especially on the 0.42 $Å^{-1}$ line resulting from the lateral packing of the nanotubes with a periodicity of ~17 Å. No peaks due to ^{40}Ar are expected given its small σ.

The experimental results have recently been reported in Ref. 26. In summary, the 0.42 $Å^{-1}$ diffraction peak was separated from the steep background by subtracting a polynomial of order three [see Fig. 6(a)] and fitted with a Gaussian function as shown in Fig. 6(b). No measurable modification of the diffraction peak is observed upon ^{40}Ar adsorption for all doses (0.7 and 2.7 mmol/g). However, a slight increase of the intensity and a shift towards smaller Q is observed upon adsorption of 0.7 mmol/g of ^{36}Ar and, more importantly, a large increase of the intensity and a sizeable shift by 0.015 $Å^{-1}$ is obtained for the largest dose (2.7 mmol/g) of ^{36}Ar. This would correspond to an "effective" increase of about 3% of the bundle lattice parameter, which is not seen upon ^{40}Ar adsorption for the same dose.

Note that the two doses correspond to the filling of the grooves and the widest interstitial channels (0.7 mmol/g) and to the completion of the rounded outer parts of the bundles (2.7 mmol/g), respectively. The conclusion of this experimental study is straightforward. The apparent dilation comes mainly from the adsorbates located on the outer surface of the bundles. Hence, the overall hexagonal arrangement of the nanotubes into bundles is preserved during adsorption, with no appreciable modification of its lattice parameter. Figure 6(c) shows the results of calculations for two doses, grooves filled and grooves and surface loaded with ^{36}Ar, without any modification of the nanotube substrate (bundle lattice spacing).[26] The experimentally observed peak shift and intensity increase is reproduced. More sophisticated nanotube bundle models with different diameter tubes[36] (to be discussed in the next section) show that populating the interstitial channels causes a local deforma-

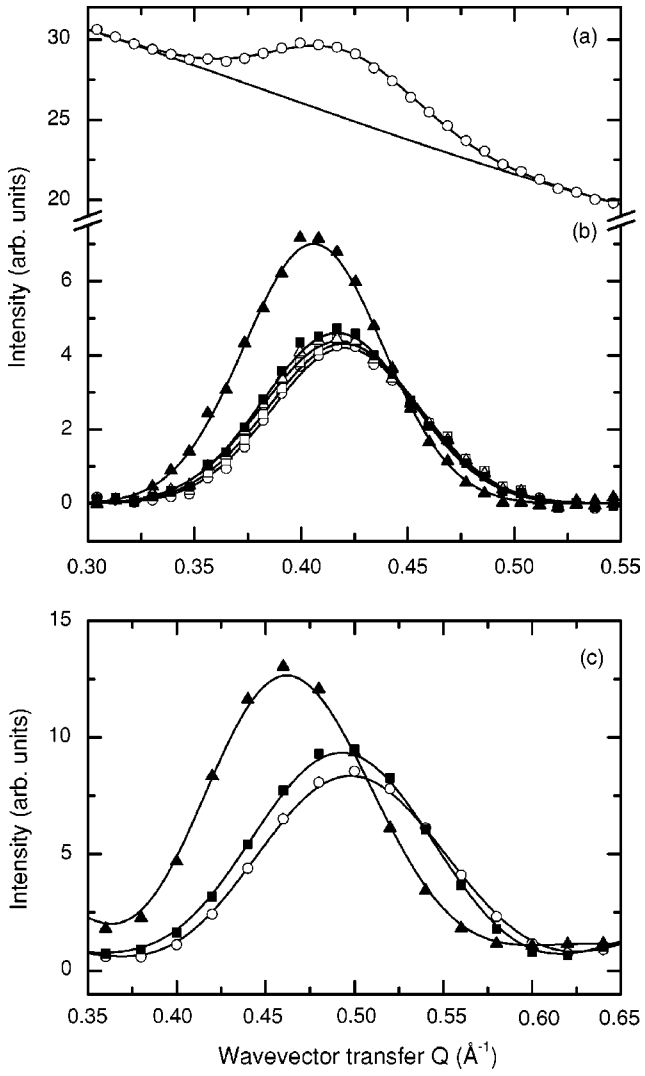

FIG. 6. (a) Neutron diffraction spectrum of the bare SWNTB sample in the vicinity of the (10) bundle lattice peak fitted by the sum of a polynomial of order three (background) and a Gaussian peak (solid lines). (b) Diffraction spectra (after background removal) of the bare SWNTB sample (open circles) and after adsorption of 0.7 and 2.7 mmol/g (squares and upper triangles, respectively) of ^{36}Ar (filled symbols) and ^{40}Ar (open symbols). The solid lines are Gaussian fits to the data. Note that a major shift and a concomitant intensity increase is observed only for the highest dose of ^{36}Ar. (c) (10) diffraction peak obtained from a simulation of a bare seven (10,10)-SWNT bundle (open circles) and after ^{36}Ar adsorption. The two ^{36}Ar coverages correspond to the filling of the grooves (solid squares) and the complete coverage of the outer surface layer (solid triangles) and can thus be compared to the spectra (same symbols) in (b). Solid lines are guides to the eye. Again, an important shift is only observed for the largest dose, i.e., after complete coverage of the outer surface of the bundle.

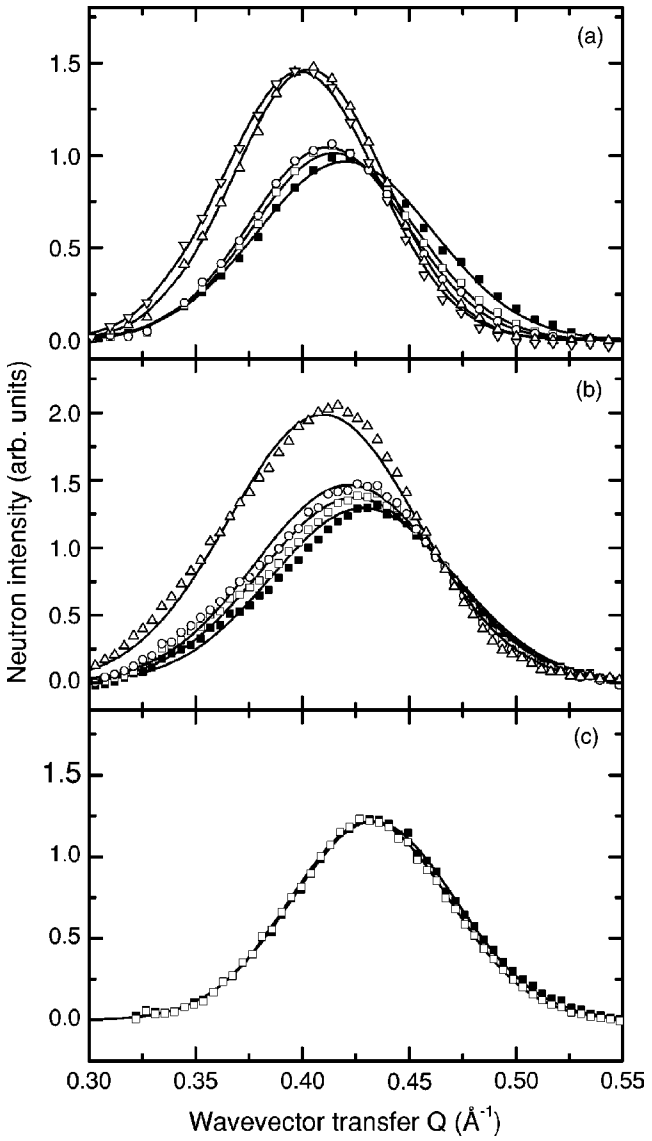

FIG. 7. Diffraction spectra (after polynomial background removal) in the vicinity of the (10) bundle lattice peak for the bare SWNTB sample (filled squares) and after adsorption of the several doses given in Table II (open symbols) of CD_4 (a), O_2 (b), and CO_2 (c). The solid lines are Gaussian fits to the data. With increasing adsorbed amount the peak intensity increases, whereas a noticeable peak shift is only observed for the highest doses in (a) and (b), corresponding to the complete coverage of the outer surface of the bundles.

tion of the nanotubes around the adsorbates without significant expansion of the bundle.

A similar *apparent* shift of the 0.42 Å^{-1} peak to lower Q-values is also observed by neutron diffraction for CD_4[5,36] and for O_2, but, again, mainly upon adsorption on the external bundle surface at higher coverages (Fig. 7). For D_2 we observe no sizeable shift of the 0.42 Å^{-1} peak at all. Indeed, computer simulations similar to those described in Ref. 36, reveal that the shift is much smaller and close to the experimental resolution. This is related to the smaller size of the D_2 molecule as compared to Ar and CD_4. A shift of the (1,0) bundle lattice peak has previously been measured by X-ray diffraction for O_2 and N_2[13] and has been attributed to a *real* dilation of the nanotube bundles induced upon adsorption into the interstitial channels. Our results show that the *apparent* dilation is due mainly to the diffraction arising from adsorbates located on the outer part of the surface at a finite binding distance away from the nanotube skeleton, thus forming an expanded envelope around the hexagonal bundle lattice. This, together with the cross interference between the adsorbates and the nanotube lattice gives rise to a shift of the bundle lattice Bragg peaks towards lower Q-values.

The absence of a peak shift to within $\Delta Q \lesssim 0.002$ Å^{-1} for ^{40}Ar doses sets an upper limit for the overall bundle swelling of $\lesssim 0.5\%$. This value is much smaller than the 2% predicted to be required for stable adsorption into the interstitial channels (IC) in a *homogeneous* bundle.[17] In reality, however, the bundles are not homogeneous and will contain a certain fraction of "wide" ICs (see Fig. 1) which may still be populated by Ar or other species without leading to a sizeable *overall* swelling of the bundle.[36] Therefore, our results are not in contradiction with the thermodynamic data (Sec. II A), which indicate that some of the widest interstitial channels must be occupied during the initial stage of adsorption.

C. Computer simulation

To guide the interpretation of the experimental data, we have calculated the equilibrium configurations and the corresponding diffraction patterns, as described in detail in Ref. 36, for several doses of adsorbates on a heterogeneous hexagonal bundle composed of 19 nanotubes. These calculations are based on empirical force-fields and can reproduce semiquantitatively the thermodynamic data as well as the diffraction patterns. The *heterogeneous* bundle used in the simulation was constructed from 19 nanotubes of (n,n) armchair configuration with n varying between 8 and 12 according to a Gaussian distribution of nanotube diameters with standard deviation $\sigma = 1.06$ Å. The adsorption of both methane and argon proceeds first in the groove sites (G) and in some of the widest interstitial channels (IC) and then on the curved outer surface (S) of the bundles (see Fig. 1). The binding energies of CD_4 adsorbed on the heterogeneous 19-tube bundle have already been reported in Ref. 36 and are not duplicated here. They are in good agreement with the experimental values summarized in Table I.

From the stable configuration of the adsorbed molecules, the adsorption energy, the pair correlation function $g(r)$ and the corresponding diffraction pattern can be calculated. As an example, two coverages of Ar adsorbed on the above model bundle have been studied. They correspond to the top of the first and second steps in the adsorption isotherm shown in Fig. 2. At the lower coverage, only the G and some of the IC sites are filled, whereas at the higher coverage all of the S sites are also occupied. The calculated $g(r)$ and the diffraction patterns are represented in Figs. 8 and 9, respectively. The Ar-Ar correlation functions exhibit a well-defined first-neighbor distance of 3.9 Å and the corresponding second-neighbor distance of 7.8 Å [Fig. 8(a)] for adsorption in the form of linear chains in the IC and G sites. The small peak at 6 Å corresponds to the closest Ar-Ar distance between inter-

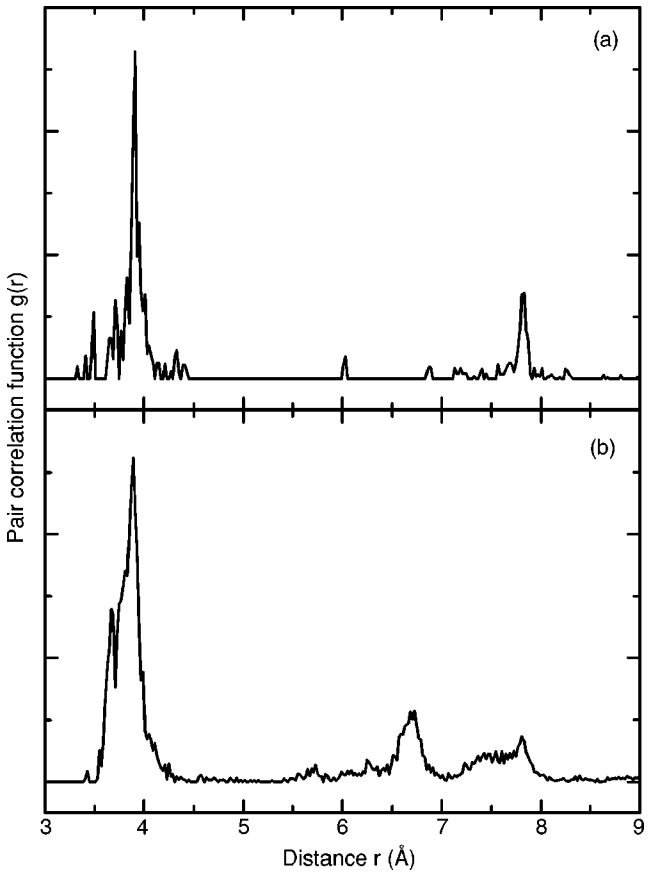

FIG. 8. Pair correlation functions for Ar on SWNTBs (a) for some IC and all G sites populated with linear chains and (b) for IC, G, and S sites populated. The peak at 6.7 Å in (b) is characteristic of hexagonal Ar packing on the outer bundle surface (S sites).

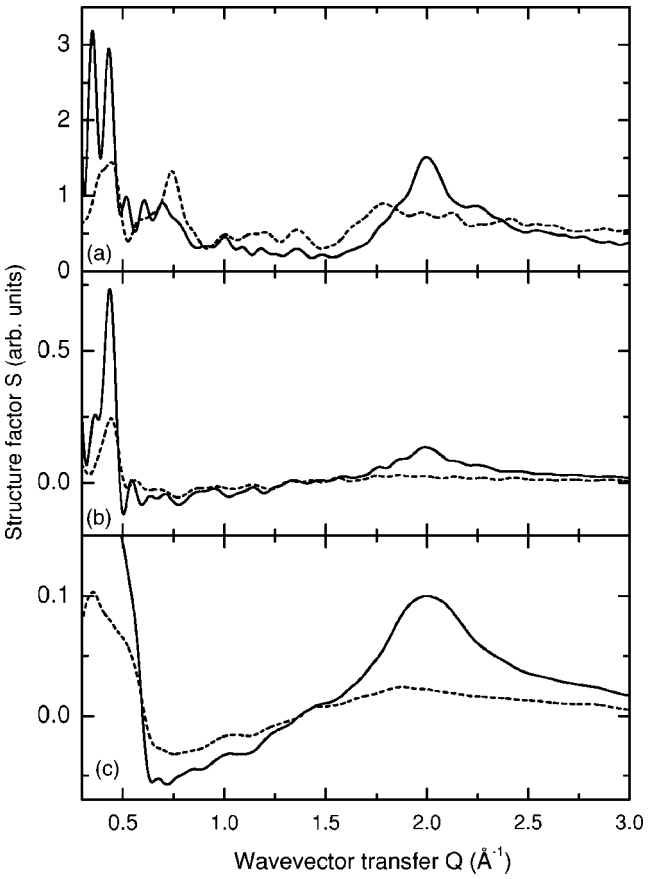

FIG. 9. Calculated diffraction patterns for Ar adsorbed on SWNTBs at two doses: some IC and all G sites populated (broken lines) and some IC, all G and S sites populated (solid lines). (a) Diffraction from the adsorbed Ar atoms, only (no C skeleton). The spectrum reveals a pronounced rise at 1.7 Å^{-1} caused by the linear chains formed on the G and IC sites, whereas the hexagonal packing on S sites gives a well-defined peak at 2.0 Å^{-1}. (b) Difference diffraction patterns obtained by subtracting the bare SWNTB spectrum from the total diffraction spectrum (Ar+SWNTB). (c) Additional smoothing of the spectrum in (b) with a Gaussian function for comparison with the experimental data shown in Fig. 5(a).

stitial chains and longer interchain separations are found above 7 Å. In Fig. 8(b), populating the surface sites gives rise to a hexagonal adsorbate structure (one side of each hexagon being an Ar-Ar vector in a groove) and a shorter second-neighbor distance of $\sqrt{3}\times 3.9$ Å. Similar results are obtained for methane, although the adsorbate structures exhibit disorder due to the rotational motion of the methane molecules (as can be seen in the snapshots of the simulated structures as shown, e.g., in Fig. 3 of Ref. 36) and the peaks in the pair correlation functions are broader than for Ar.

Strictly speaking, the first maximum in the $g(r)$ function provides information on the nearest-neighbor distance within the adsorbate, but not on the medium- or long-range order. The latter can be better judged from the calculated diffraction patterns. We focus here on the scattering vector range between 1.5 and 2.2 Å^{-1} where the adsorbate packing in either linear chains or quasi-hexagonal arrays can be detected. To this end, the diffraction spectra (structure factors) were calculated on the basis of the simulated structures also used to extract the pair correlation functions in Fig. 8. The clearest diffraction signature of linear and hexagonal packing is seen in the diffraction patterns calculated for the adsorbate [Fig. 9(a)]. The dashed curve corresponds to a low coverage of Ar, for which only linear chains are present, and a pronounced rise in the diffracted intensity is seen at 1.7 Å^{-1}. The solid curve corresponds to a higher coverage of Ar, with hexagonal packing on the nanotube surfaces, and, accordingly, a well-defined maximum is observed at 2.0 Å^{-1}. Figure 9(b) shows the *difference* between the calculated spectra including the adsorbed Ar atoms and the raw SWNTB diffraction spectra obtained without Ar. Results for the same two Ar coverages considered in Fig. 9(a) are shown. The signatures of 1D and 2D packing (diffraction features at 1.7 and 2.0 Å^{-1}, respectively) are less clear due to the C-Ar cross-terms in the total diffracted intensity, which are not removed on subtracting the background (see below). For a straightforward comparison with the data in Fig. 5, Fig. 9(c) shows the curves of Fig. 9(b) after convolution with a Gaussian function with FWHM=0.1 Å^{-1}. This resolution or transfer function describes the imperfect ordering and bundle size distribution; its width corresponds to the experimentally observed broadening of the diffraction features observed on the bare SWNTB sample.

The adsorption of the Ar molecules results in a strong modification of the diffracted intensities, namely a drop between 0.5 and 1.5 $Å^{-1}$ and an increase between 1.5 and 2.5 $Å^{-1}$. Several oscillations can be seen. They arise from the finite size of the single bundle used in the simulation and are also present in the calculated diffraction spectrum of the bare bundle (not shown here). In addition, an important part of the diffracted intensity comes from cross-interference effects between the adsorbed atoms and the carbon skeleton as already pointed out in Ref. 36 and Sec. II B 1. The overall increase of the intensity in the *Q*-range between 1.5 and 2.5 $Å^{-1}$ stems from the medium-range order of the Ar atoms. The absence of narrow diffraction peaks in Fig. 9 shows that there is no true long-range order among the adsorbates. We observe an upward shift in *Q* of the intensity maximum when the coverage increases from the first to the second riser. This shift in Q of about 10% is consistent with the initial condensation of linear chains in the G and IC sites, followed at higher coverage by the formation of pseudo-hexagonal patches on the outer bundle surface. Indeed, the first order Bragg peak of a 2D hexagonal lattice is located at a $2/\sqrt{3}$ times higher *Q* value than that of a 1D chain with the same nearest-neighbor spacing.

While adsorption in G and S sites does not induce any deformation of the nanotube bundle, simulations show that adsorption in the larger, energetically favorable IC sites causes a local deformation of the nanotubes without, however, inducing a significant overall expansion of the bundle. The amplitude of this deformation depends on the size of the adsorbate. For methane, the largest adsorbate, the bundle deformation gives rise to a small shift of 0.006 $Å^{-1}$ of the hexagonal bundle lattice peak. For argon, the shift is half as big and therefore experimentally unobservable (as was found with ^{40}Ar), and for D_2, the smallest adsorbate, the calculated peak shift is zero for all doses of D_2.

The simulation results are in semi-quantitative agreement with the trend observed in the experimental diffraction patterns for Ar, D_2, and CD_4 presented in Fig. 5. Note that the same kind of calculated diffraction patterns have been reported in Ref. 36 for the adsorption of various doses of CD_4 on *homogeneous* and *heterogeneous* SWNTB samples. The new results reported here show that the simulation yields the same qualitative trends in the case of Ar (mainly), D_2, and CO_2 on a *heterogeneous* bundle. This demonstrates the robustness of the conclusions drawn here. However, we cannot rule out the existence of rather wide ICs permitting in our bundle the adsorption of zig-zag chains as proposed in Ref. 5. In addition, the experimental SWNTB diffraction pattern might exhibit diffraction signatures due to the presence of graphitized carbon impurities, on which molecules can adsorb in small pseudo-hexagonal patches. Such contributions are not taken into account in the present simulation, but could give rise to a non-negligible signal in the diffraction spectra.

III. CONCLUSIONS

Although our SWNTB sample is heterogeneous and ill-crystallized, the combination of thermodynamic, neutron diffraction, and computer simulation studies allows a good description of the adsorption phenomena on this sample. We were able to localize the adsorption sites and estimate the amount adsorbed on the different sites. We have shown that the adsorption scenario is the same, on our sample, for the different gases reported here—except for CO_2. The variation of the adsorption energy is measured as a function of coverage and the various energies are qualitatively assigned to the different sites: the more strongly binding sites being the grooves (G) and some of the interstitial channels (IC) and the less strongly binding sites being those on the curved outer surfaces (S). The linear chains in the G and IC sites as well as the pseudo-hexagonal patches on the S sites are poorly organized and the adsorbates exhibit only a medium-range order. Finally, in our case, the adsorption does not modify the average hexagonal arrangement of the nanotubes within each bundle nor does it result in a sizeable overall swelling of these bundles.

ACKNOWLEDGMENTS

The authors thank N. Dufau and Y. Grillet for performing the calorimetric measurements. T.W., M.D.P., and O.E.V. acknowledge support from the USA National Science Foundation through Grant No. DMR 0115663.

*Electronic address: peter.zeppenfeld@jku.at
†Deceased.
‡Permanent address: Department of Physics, Makassar State University, 90222 Makassar, Indonesia.

[1] M.M. Calbi, M.W. Cole, S.M. Gatica, M.J. Bojan, and G. Stan, Rev. Mod. Phys. **73**, 857 (2001).
[2] M. Muris, N. Dufau, M. Bienfait, N. Dupont-Pavlovsky, Y. Grillet, and J.-P. Palmari, Langmuir **16**, 7019 (2000).
[3] M. Bienfait, B. Asmussen, M. Johnson, and P. Zeppenfeld, Surf. Sci. **460**, 243 (2000).
[4] M. Bienfait, B. Asmussen, P. Zeppenfeld, W. Press, J.-P. Palmari, M. Johnson, C. Journet, P. Bernier, K. Méténier, S. Bonnamy, and N. Dupont-Pavlovsky, Physica B **301**, 292 (2001).
[5] M. Muris, M. Bienfait, P. Zeppenfeld, N. Dupont-Pavlovsky, M. Johnson, O.E. Vilches, and T. Wilson, Appl. Phys. A: Mater. Sci. Process. **74**, S1293 (2002).
[6] T. Wilson, A. Tyburski, M.R. De Pies, O.E. Vilches, D. Becquet, and M. Bienfait, J. Low Temp. Phys. **126**, 403 (2002).
[7] W. Teizer, R.B. Hallock, E. Dujardin, and T.W. Ebbesen, Phys. Rev. Lett. **82**, 5305 (1999); *ibid.* **84**, 1844(E) (2000).
[8] S. Talapatra, A.Z. Zambano, S.E. Weber, and A.D. Migone, Phys. Rev. Lett. **85**, 138 (2000).
[9] A. Kuznetsova, J. Yates, Jr., J. Lin, and R.E. Smalley, J. Chem. Phys. **112**, 9590 (2000).
[10] V.S. Simonyan, J.K. Johnson, A. Kuznetsova, and J. Yates, Jr., J. Chem. Phys. **114**, 4180 (2001).

[11] S.E. Weber, S. Talapatra, C. Journet, A. Zambano, and A.D. Migone, Phys. Rev. B **61**, 13150 (2000).
[12] A.J. Zambano, S. Talapatra, and A.D. Migone, Phys. Rev. B **64**, 075415 (2001).
[13] A. Fujiwara, K. Ishii, H. Suematsu, H. Kataura, Y. Maniwa, S. Suzuki, and Y. Achiba, Chem. Phys. Lett. **336**, 205 (2001).
[14] M. Muris, N. Dupont-Pavlovsky, M. Bienfait, and P. Zeppenfeld, Surf. Sci. **492**, 67 (2001).
[15] S. Talapatra and A.D. Migone, Phys. Rev. Lett. **87**, 206106 (2001).
[16] S. Talapatra and A.D. Migone, Phys. Rev. B **65**, 045416 (2002).
[17] M.M. Calbi, F. Toigo, and M.W. Cole, Phys. Rev. Lett. **86**, 5062 (2001). See also G. Stan, M.J. Bojan, S. Curtarolo, S.M. Gatica, and M.W. Cole, Phys. Rev. B **62**, 2173 (2000) for calculated binding energies at various sites on a bundle. Stan *et al.* predict a much larger binding to the G sites than to the IC sites for Ar, even with bundle dilation.
[18] S.M. Gatica, M.J. Bojan, G. Stan, and M.W. Cole, J. Chem. Phys. **114**, 3765 (2001).
[19] M.M. Calbi, S.M. Gatica, M.J. Bojan, and M.W. Cole, J. Chem. Phys. **115**, 9975 (2001).
[20] A.D. Migone and S. Talapatra, in *Encyclopedia of Nanoscience and Technology*, edited by H.S. Nalwa (American Scientific Publishers, Washington, D.C., 2004), in press.
[21] M.S. Dresselhaus, K.A. Williams, and P.C. Eklund, MRS Bull. **24**, 45 (1999).
[22] A.C. Dillon and M.J. Heben, Appl. Phys. A: Mater. Sci. Process. **72**, 133 (2001).
[23] Q. Wang, S.R. Challa, D.S. Sholl, and J.K. Johnson, Phys. Rev. Lett. **82**, 956 (1999).
[24] S.R. Challa, D.S. Sholl, and J.K. Johnson, Phys. Rev. B **63**, 245419 (2001).
[25] M.C. Gordillo, J. Boronat, and J. Casulleras, Phys. Rev. Lett. **85**, 2348 (2000).
[26] M. Bienfait, P. Zeppenfeld, N. Dupont-Pavlovsky, J.-P. Palmari, M.R. Johnson, T. Wilson, M. De Pies, and O.E. Vilches, Phys. Rev. Lett. **91**, 035503 (2003).
[27] J. Stoltenberg and O.E. Vilches, Phys. Rev. B **22**, 2920 (1980).
[28] M.F. Toney, R.D. Diehl, and S.C. Fain, Jr., Phys. Rev. B **27**, 6413 (1983).
[29] M.F. Toney and S.C. Fain, Jr., Phys. Rev. B **30**, 1115 (1984).
[30] J.P. Mc Tague and M. Nielsen, Phys. Rev. Lett. **37**, 596 (1976).
[31] M. Nielsen and J.P. Mc Tague, Phys. Rev. B **19**, 3096 (1979).
[32] P.W. Stephens, P.A. Heiney, R.J. Birgeneau, P.M. Horn, J. Stoltenberg, and O.E. Vilches, Phys. Rev. Lett. **45**, 1959 (1980).
[33] P.G. Collins, K. Bradley, M. Ishigami, and A. Zettl, Science **287**, 1801 (2000).
[34] S.H. Jhi, S.G. Louie, and M.L. Cohen, Phys. Rev. Lett. **85**, 1710 (2000).
[35] A. Terlain and Y. Lahrer, Surf. Sci. **125**, 304 (1983).
[36] M.R. Johnson, S. Rols, P. Wass, M. Muris, M. Bienfait, P. Zeppenfeld, and N. Dupont-Pavlovsky, Chem. Phys. **293**, 217 (2003).
[37] C. Journet, W.K. Maser, P. Bernier, A. Loiseau, M. Lamy de la Chapelle, S. Lefrant, P. Deniard, R. Lee, and J.E. Fisher, Nature (London) **388**, 756 (1997).
[38] S. Rols, R. Almairac, L. Henrard, E. Anglaret, and J.-L. Sauvajol, Eur. Phys. J.: Appl. Phys. **10**, 263 (1999).
[39] P. Zeppenfeld (unpublished).
[40] Y. Grillet, F. Rouquerol, and J. Rouquerol, J. Colloid Interface Sci. **70**, 239 (1979).
[41] C. Letoquart, F. Rouquerol, and J. Rouquerol, J. Chim. Phys. Phys.-Chim. Biol., **70**, 559 (1973).
[42] M. Nielsen, J.P. Mc Tague, and W. Ellenson, J. Phys. (Paris) **38**, C4 (1977).
[43] H. Freimuth, H. Wiechert, H.P. Schildberg, and H.J. Lauter, Phys. Rev. B **42**, 587 (1990).
[44] H. Taub, K. Carneiro, J.K. Kjems, L. Passell, and J.P. Mc Tague, Phys. Rev. B **16**, 4551 (1977).
[45] J.-M. Gay, A. Dutheil, J. Krim, and J. Suzanne, Surf. Sci. **177**, 25 (1986).
[46] W. Shi and J.K. Johnson, Phys. Rev. Lett. **91**, 015504 (2003).
[47] K. Masenelli-Varlot, E. McRae, and N. Dupont-Pavlovsky, Appl. Surf. Sci. **196**, 209 (2002).
[48] G. Vidali, G. Ihm, H.Y. Kim, and M.W. Cole, Surf. Sci. Rep. **12**, 135 (1991).
[49] J. Dericbourg, Surf. Sci. **59**, 554 (1976).
[50] H. Ulbricht, G. Moos, and T. Hertel, Phys. Rev. B **66**, 075404 (2002).
[51] 0.9 kJ/mol and 1.3 kJ/mol at 20 K for H_2 and D_2, respectively: P.C. Sours, *Hydrogen Properties for Fusion* (University of California Press, Berkeley, CA, 1986), p. 112.